Chinese Journal of
POLYMER SCIENCE

RESEARCH ARTICLE

https://doi.org/10.1007/s10118-026-3782-7
Chinese J. Polym. Sci.

Self-healing, High-resilience, and UV-curable Polyurethane-urea Elastomers Enabled by Dual Crosslinked Networks

Meng-Yuan Cai, Sao Su, Wen-Tao Du, Rui-Jie Xu*, and Hong-Ping Xiang*

School of Materials and Energy, Guangdong University of Technology, Guangzhou 510006, China

Electronic Supplementary Information

Abstract Self-healing polyurethane (PU) elastomers will greatly extend the service life of key components, reduce maintenance costs, and promote sustainability. However, dense hydrogen bonds cannot quickly recover after stretching, causing permanent deformation, while high-temperature and long-duration curing are required for their crosslinking. Therefore, dual crosslinked networks are designed herein to achieve self-healable, high-resilience and UV-curable polyurethane-urea elastomers (PUU-SS-Zn), using polycarbonate diol (PCDL) as the soft segment for entropic elasticity, cystamine (Cy) as a chain extender for disulfide bonds and urea-linked hydrogen bonds, 2-hydroxyethyl acrylate (HEA) as end-capping groups for rapid UV-curing, $ZnCl_2$ for metal coordination bonds. The resultant elastomers are UV-cured within 100 s, exhibit a transmittance >92%, tensile strength of 11.8 MPa, and elongation at break of 2423%. More importantly, it achieves nearly 100% resilience at 500% strain within 5 s, realizes 99.6% resilience at 1000% strain within 5 min, and maintains 90.2% after multiple cycles. Surface scratches disappear within 30 min at 60 °C, and the self-healing efficiency reaches 93% after 8 h at 80 °C. This self-healable, high-resilience and UV-curable polyurethane-urea elastomer shows great application potentials in flexible sensors and wearable devices.

Keywords Polyurethane-urea elastomer; UV-curing; High resilience; Self-healing; Dual crosslinked network

Citation: Cai, M. Y.; Su, S.; Du, W. T.; Xu, R. J.; Xiang, H. P. Self-healing, high-resilience, and UV-curable polyurethane-urea elastomers enabled by dual crosslinked networks. *Chinese J. Polym. Sci.* https://doi.org/10.1007/s10118-026-3782-7

INTRODUCTION

Polyurethane (PU) elastomers, a class of polymers with strong molecular designability, provide an ideal molecular platform for tunable mechanical properties, self-healing, and recyclability by adjusting the microphase separation structure of soft and hard segments.[1–4] This platform strongly supports the rapid development of flexible electronics,[5] soft robotics,[6] and smart wearable devices.[7] However, current PU elastomers often achieve stiffness, toughness, and self-healing capability while neglecting rapid resilience[8] and fast curing.[9] Rapid resilience is crucial for improving the response speed and ensuring signal stability, whereas fast curing offers significant advantages in terms of low energy consumption and high efficiency for future material manufacturing. Therefore, endowing PU elastomers with both high resilience and fast curing remains a key challenge that urgently needs to be addressed in this field.

To develop PU elastomers with ultrahigh toughness, rapid resilience, and intrinsic self-healing properties, various soft segments have been explored. A chemically crosslinked polyurethane-urea elastomer synthesized using poly(propylene glycol) and tolylene 2,4-diisocyanate terminated (PPGTD) as the soft segment can recover 700% strain within 2 h and heal surface scratches under *N*,*N*-dimethylformamide assistance within 1 h.[10] A sliding semi-crystalline dynamic hydrogen bonding array was designed using bis(3-aminopropyl)-terminated poly(dimethylsiloxane) (PDMS-NH_2) as the soft segment, achieving an elastomer with ultrahigh elongation at break (2880%) and skin-friendly healing temperature.[11]

Beyond soft segment selection, dynamic covalent bonds (*e.g.*, Diels-Alder,[12,13] disulfide,[14] acylhydrazone bonds,[15] or imine bonds), and strong physical interactions (*e.g.*, multiple hydrogen bonds or metal coordination[16]) have also been introduced during hard segment design to achieve high resilience and self-healing. A novel polyurethane elastomer is developed, consisting of ascorbic acid-based chemodynamic covalent adaptive networks, achieving a tensile strength of 47.9 MPa, an elongation at break of 1746%, and fast self-healing within approximately 1 s.[4] By introducing 1,4-benzoquinone dioxime as a chain extender, the oxime-urethane bond and hydrogen bond confer room-temperature self-healing and recycling properties to a polyurethane elastomer, achieving a tensile strength of 30.3 MPa and an elongation at break of 1114%. The elastomer recovers 900% of the strain within 10 min, and scratches heal at room temperature within 2 h.[17] A polyurethane-urea elastomer was synthesized by

* Corresponding authors, E-mail: Xuruijie@gdut.edu.cn (R.J.X.)
E-mail: Xianghongping@gdut.edu.cn (H.P.X.)
Received May 6, 2026; Accepted June 10, 2026; Published online August 28, 2026

incorporating aromatic disulfide bonds and multiple hydrogen bonds, showing a tensile strength of 14.08 MPa. It recovers 300% strain with a 10 s hold and 10 s relaxation, and exhibits a room-temperature self-healing efficiency of 81%.[18] Through rational soft/hard segment design and the synergistic introduction of multiple hydrogen bonds and other dynamic bonds, these elastomers achieve excellent multifunctional synergy, extending service life and reducing maintenance costs. However, their synthesis and curing face challenges, such as multi-step reactions, long cycles, high-temperature curing (>80 °C) unsuitable for heat-sensitive substrates, and curing times ranging from hours to days.

UV-curing technology enables rapid curing at room temperature with low energy consumption, solvent-free manufacturing, and patternable fabrication, making it suitable for temperature-sensitive flexible substrates and complex devices.[19] A 3D-printable and dynamically recyclable polyurethane elastomer exhibited a tensile strength of 3.38 MPa, an elongation at break of 1425%, and a self-healing efficiency of 95.86% after healing at 50 °C for 6 h.[20] A UV-curable silane-modified polyurethane acrylate (PUA) for flexible sensing revealed a tensile strength of 8.67 MPa and an elongation at break of 378%.[21] Currently, UV-curing polyurethanes that combine self-healing and rapid resilience are rarely reported. Achieving rapid UV-curing while constructing a dynamic network that can reversibly break and recombine for self-healing and rapidly recombine to eliminate residual strain remains a key challenge that needs to be addressed in this field.

In this study, a UV-curable polyurethane elastomer (PUU-SS25%-Zn1wt%) with ultrahigh resilience and self-healing efficiency was successfully designed and prepared. PCDL was used as the soft segment to provide entropic elasticity. Cy serves as a chain extender to introduce dynamic disulfide bonds and urea-linked hydrogen bonds, whereas $ZnCl_2$ is added to form reversible metal coordination bonds that act as sacrificial crosslinks. Ultraviolet curing was used to construct a stable permanent covalent network. The dual networks enabled nearly complete recovery within 5 s after 500% strain, achieving an elastic recovery rate of 99.6% within 5 min after 1000% strain, and maintaining 90.2% after five cycles. Self-healing efficiency reached 93% after thermal treatment at 80 °C for 2 h. The material also exhibited high transparency (>92%), a tensile strength of 11.8 MPa, and an ultrahigh elongation at break of 2423%. This work provides a new design strategy for UV-curable, self-healing polyurethane-urea elastomers for flexible electronics, intelligent sensing, and biomedical engineering.

EXPERIMENTAL

Materials

Polycarbonate diol (PCDL) was purchased from Ube Kosan Co., Ltd. Hexamethylenediamine (HDA), cystamine (Cy), 4,4'-dicyclohexylmethane diisocyanate (HMDI), hydroxyethyl acrylate (HEA), ethyl acetate, isopropyl alcohol (IPA), zinc chloride ($ZnCl_2$), and ethyl 2,4,6-trimethylbenzoylphenyl phosphonate (TPO-L) were purchased from Aladdin Biochemical Technology Co., Ltd.

Synthesis of UV-curing Polyurethane-urea Elastomers (PUU-SS-Zn)

The Cy content significantly affected the resilience and self-healing properties of the UV-curable polyurethane. Samples with varying Cy contents were denoted as PUU-SS*x*%, where *x* was the mole percentage of Cy relative to the PCDL soft segment (see Table S1 for the formulations in the electronic supplementary information, ESI). The preparation process is illustrated in Figs. 1a and 1b), with the synthesis of PUU-SS25% described below as an example.

Dehydrated PCDL (30 g, 15 mmol, 1.0 equiv.) and ethyl acetate (20 g) were added to a 250 mL four-necked flask and stirred at 60 °C for 30 min under N_2 to form a homogeneous solution. HMDI (6.61 g, 25.2 mmol, 1.0 equiv.) in ethyl acetate (10 g) was added dropwise at 0.5 mL/min. Subsequently, a trace amount of DBTDL catalyst (0.05 wt%) was added, and the reaction proceeded at 60 °C for 3 h to complete the prepolymerization. Cy (0.57 g, 3.74 mmol, 1.0 equiv.) was added dropwise at room temperature with ethyl acetate to control viscosity. The reaction continued for 2 h. Then, HEA (4.494 g, 38.7 mmol, 1.2 equiv.) in ethyl acetate (10 g) was added dropwise at 0.5 mL/min, and the reaction continued at 60 °C for 3 h.

UV-curing of Elastomers

The viscous product was mixed with 2 wt% photoinitiator, ultrasonicated for 15 min, poured into a PTFE mold, and kept in the dark at room temperature for 24 h to evaporate the solvent. It was then cured using a UV belt-type curing machine (LT-UV102) for 100 s to obtain PUU-SS25%. To prepare PUU-SS25%-Zn1wt%, the polymer was blended with 1 wt% $ZnCl_2$ and 2 wt% photoinitiator, stirred, ultrasonicated for 30 min, and then UV cured (see Table S2 for other formulations in ESI).

Characterization

PUU-SS was characterized using FTIR (Thermo Fisher Nicolet iS50) over 4000–400 cm^{-1} (resolution: 4 cm^{-1}, 32 scans). The photopolymerization conversion (C_t) of acryloyl double bonds was monitored by real-time FTIR using a 405 nm UV-LED (30 mW/cm^2). C_t was calculated using Eq. (1) based on the C=C peak change at 1600 cm^{-1}.

$$C_t = \frac{A_0 - A_t}{A_0} \times 100\% \quad (1)$$

A_0 and A_t are the peak areas of acrylate at 1600 cm^{-1} before and after UV irradiation for different times, respectively.

Tensile tests were performed on a universal testing machine (STD500, 500 N sensor) using dumbbell-shaped specimens (50 mm × 4 mm × 2 mm). The width and thickness were measured with a Vernier caliper (0.01 mm accuracy).

The gauge length was 10 mm and the strain rate was 100 mm/min. The hardness was measured using a Shore A dynamometer. A 1 kg of load was applied for 15 s, and five measurements were taken at intervals of ≥6 mm. The light transmittance from 400 nm to 800 nm was measured using a Shimadzu UV-2450 spectrophotometer according to ASTM D1003-13. Crosslinking density was determined using the equilibrium swelling method. About 0.2 g of sample was immersed in 25 mL of toluene at room temperature. After 24 h, toluene was replaced and the sample was immersed for an-

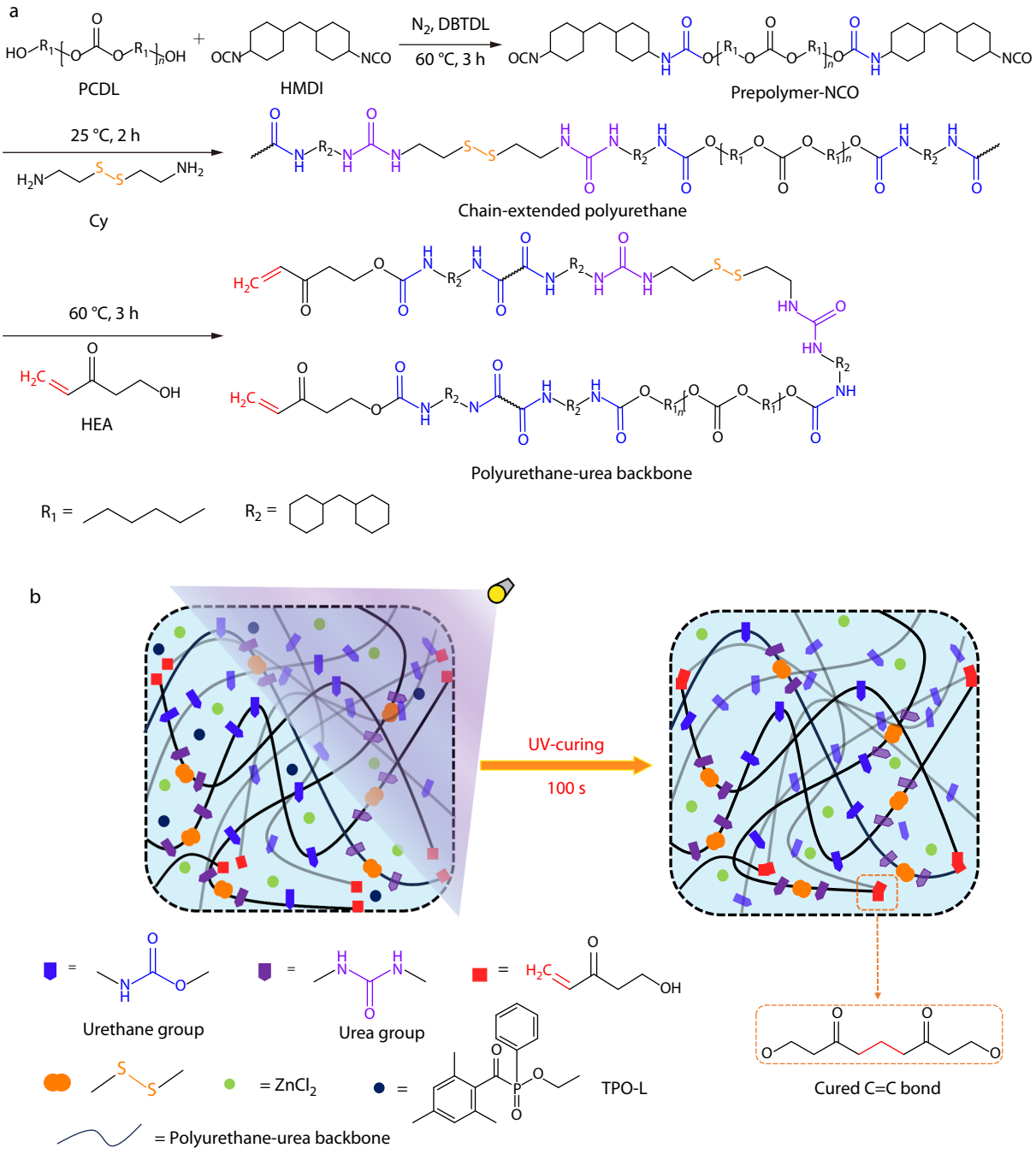

Fig. 1 (a) Synthesis process for PUU-SS prepolymer; (b) UV-curing and crosslinking network structure of PUU-SS*x*%-Zn*y*%.

other 48 h. The swollen samples were wiped dry, weighed, dried at 60 °C for 4 h, and reweighed. The crosslinking density was calculated using Eqs. (2) and (3), respectively.

$$\phi = \frac{\frac{W_2}{\rho_s}}{\frac{(W_1 - W_0)}{\rho_0} + \frac{W_2}{\rho_s}} \quad (2)$$

$$v = -\frac{\ln(1-\phi) + \phi + \chi\phi^2}{V_0\left(\phi^{\frac{1}{3}} - \frac{\phi}{2}\right)} \quad (3)$$

where ϕ is the volume fraction of the PUU-SS*x*%-Zn*y*% sample under equilibrium swelling conditions; W_0, W_1, and W_2 represent the original, swollen, and dried masses of the sample (g), respectively, ρ_s and ρ_0 are the densities of the sample before swelling and toluene (0.87 g/cm^3), respectively; V is the volume fraction; v is the cross-linking density; χ is the polymer–solvent interaction parameter (0.465[22]); and V_0 is the molar volume of toluene (105.7 cm^3/mol). Dumbbell-shaped specimens were used for repeated resilience tests. The effective gauge length was 10 mm (the initial gauge lines were marked on the parallel section of the specimen using a solvent-resistant marker). The

specimen was stretched to 100%, 500%, and 1000% strain at a rate of 100 mm/min, and then rapidly unloaded. The effective gauge length was measured after 5 min. For each strain condition, at least five parallel specimens were tested, and the results were reported as the mean ± standard deviation. The elastic recovery rate was calculated using Eq. (4).

$$R = 1 - \frac{L_{after,n} - L_0}{L_0} \times 100\% \quad (4)$$

where R represents the elastic recovery rate, $L_{after,n}$ represents the effective gauge length after stretching, followed by a 5 min rest, and L_0 represents the initial effective gauge length (10 mm).

The dynamic mechanical properties of the material were measured using a dynamic mechanical analyzer (DMA-50N, MetraviB) in tensile mode. Frequency sweep tests were conducted at 25 °C with a strain amplitude of 1% over the frequency range of 0.1–50 Hz. The relaxation time (τ) of the specimen under a 5% tensile strain was measured at different temperatures (T), and the characteristic relaxation time was calculated using Eq. (5).

$$\tau(T) = \tau_0 \exp\left(\frac{E_a}{RT}\right) \quad (5)$$

where $\tau(T)$ is the relaxation time, τ_0 is the pre-exponential factor, E_a is the activation energy, R is the gas constant (8.314 J/(mol·K)), and T is the absolute temperature.

A cyclic fatigue test resting time was applied between cycles to simulate continuous mechanical loading conditions. The energy dissipation per cycle (W_x) was recorded, and the energy dissipation retention rate ($W_{100}/W_1 \times 100\%$) was calculated. All tests were performed at room temperature (25 °C), and at least five specimens were tested for each sample to ensure the reproducibility, as evaluated using Eq.(6).

$$W = \int_{loading} \sigma d\varepsilon - \int_{unloading} \sigma d\varepsilon \quad (6)$$

where W is the hysteresis work, ε is the strain, σ is the stress, and the integration interval covers a complete cycle.

The dumbbell-shaped specimen was cut in half and the fractured surfaces were brought into contact. The specimens were heated to 80 °C for 8 h for thermal healing. After healing, tensile tests were performed using a universal testing machine. The healing efficiency was calculated by comparing the tensile properties (tensile strength and elongation at break) before and after the cutting. Additionally, an optical microscope was used to observe the scratch healing. A cross-shaped scratch was created by using a razor blade. The scratched sample was placed on a hot stage at 60 °C and the scratch morphology was examined at different time intervals. The healing performance was evaluated based on the scratch closure, and the self-healing efficiency was calculated by comparing the strength before and after healing.

RESULTS AND DISCUSSION

Structure Characterization and UV-curing of PUU-SS-Zn Elastomers

Fig. 2(a) presents the FTIR spectra during the PUU-SS25% synthesis. The disappearance of the —NCO band at 2270 cm^{-1} indicates complete isocyanate consumption. The broad band at 3350 cm^{-1} and the band at 1540 cm^{-1} confirm —NHCOO— and NH—CO—NH formation, while the C=C band at 1640 cm^{-1} confirms HEA end-capping. The cured PUU-SS25%-Zn1wt% elastomer (Fig. 2b and Fig. S1b in ESI), the broad band at 3390 cm^{-1} indicates extensive hydrogen bonding. The sharp peak at 1750 cm^{-1} (PCDL carbonate C=O) confirms the integrity of the soft segment. The peak at 1520 cm^{-1} (amide II) confirms urethane/urea linkages, and the weak peak at 650 cm^{-1} is assigned to C—S stretching from Cy. Zn^{2+} coordination with N/O atoms enhances hydrogen bonding, evidenced by peak broadening at 3350 cm^{-1} and C=O red shift from 1747 cm^{-1} to 1733 cm^{-1}. These results confirm the successful preparation of PUU-SS25%-Zn1wt%, where the permanent UV-cured covalent network coexists with a dynamic network of multiple hydrogen, disulfide, and metal coordination bonds.

As shown in Fig. 2(c) and Fig. S1(c) (in ESI), free-radical photosensitive resins were prepared by mixing 2 wt% TPO-L with polyurethanes containing different Cy contents. Acryloyl double bond conversion was measured under a 405 nm UV-LED (40 mW/cm^2). Conversion generally decreased with increasing Cy content because longer chains entangled, and unreacted acryloyl double bonds[23] froze in the cured network after initial crosslinking. The curing rate also decreased with Cy content, PUU-SS0%, and PUU-SS10% cured within 15 s, while PUU-SS30% required 110 s. Longer chains reduced the acryloyl double bonds per unit volume, lowering the collision probability. Interestingly, PUU-SS0% exhibited a lower conversion and curing rate than PUU-SS10%. This is due to its short rod-like chains, as rapid crosslinking traps unreacted acryloyl double bonds, despite high chain mobility. In contrast, PUU-SS10% achieved a higher conversion and curing rate owing to its appropriate chain length from Cy. After the addition of $ZnCl_2$, the UV-curing rate and conversion remained largely unchanged, as shown in Fig. 2(c). and Fig. S1(d) (in ESI). The bands of acryloyl double bonds decreased with irradiation time, and the trend slowed after 60 s, indicating a fast UV-curing process.[24,25] Although PUU-SS25% exhibited acryloyl double bond conversion of only 38.14%, and PUU-SS25%-Zn1wt% exhibited 34.8%, this moderate crosslinking density provided an optimal balance that enabled the material to resist deformation while dissipating energy through segmental motion, resulting in high strength and excellent toughness. As shown in Fig. 2(d), the UV-cured PUU-SS25% elastomer exhibited high transparency (about 97%), with little effect from the addition of TPO-L or $ZnCl_2$. The excellent transparency of PUU-SS25%-Zn1wt% is mainly due to the absence of aromatic structures in HMDI, PCDL, Cy, and HEA, which lack visible light absorption, conferring intrinsic transparency.[26] A uniform network with good soft/hard segment compatibility also prevents significant light scattering.

Although the transmittance slightly decreased in the 400–800 nm range, it remained above 90%, which was attributed to the minimal residual photoinitiator with good refractive index matching. Zn^{2+} coordination causes weak charge transfer absorption, mainly in the near-UV to blue region (400–450 nm). Combined with its amorphous nature, the material achieves enhanced mechanical properties *via* the metal coordination network while maintaining excellent transparency, demonstrating its potential for flexible elec-

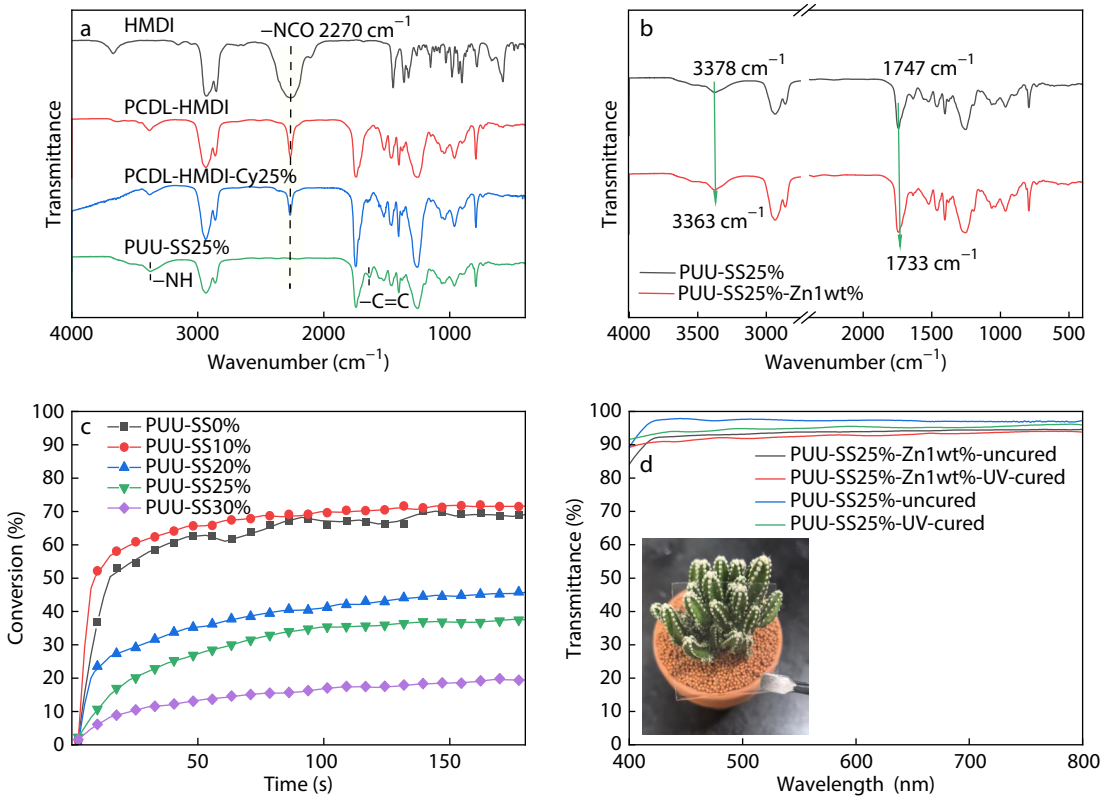

Fig. 2 (a) FTIR spectra recorded during the synthesis of PUU-SS25%; (b) FTIR spectra of PUU-SS25% and PUU-SS25%-Zn1wt%; (c) Conversion of acryloyl double bonds in different PUU-SS*x*% samples; (d) Transmission spectra of PUU-SS25%-Zn1wt% and PUU-SS25% before and after curing, and optical image of PUU-SS25%-Zn1wt% after curing (1.0 mm thick).

tronics and optical devices.

Mechanical Properties of PUU-SS-Zn Elastomers

This study aims to synthesize high-resilience polyurethanes using PCDL, PTMEG1k, PTMEG2k, HMDI, IPDI, and MDI. After HEA end-capping, UV curing was performed (Figs. S2a and S2b in ESI). PCDL2k/HMDI exhibited a synergistic effect of high strength and extensibility, making it the optimal choice. As shown in Fig. 3(a), with increasing Cy content from 0% to 25%, both tensile strength and elongation at break of the material increased synergistically, reaching optimal values at 25% (strength 6.41 MPa, elongation at break 1198%). This is attributed to the introduction of an appropriate amount of Cy, which extends the molecular chains, promotes physical entanglement and hard-segment hydrogen bonding, and constructs a more perfect physical crosslinking network. Meanwhile, moderate chain segment mobility provides favorable conditions for efficient acryloyl double-bond conversion, forming a stable covalent crosslinking network. The disulfide bonds achieve optimal mobility at this network density, effectively dissipating energy through reversible breakage and recombination, delaying crack propagation, and thus achieving simultaneous improvements in strength and elongation. When the Cy content was increased to 30%, the material properties declined sharply, exhibiting soft and slippery characteristics. This is because excessive amine groups undergo rapid reactions, leading to local over-crosslinking, forming microgel particles that create weak interfaces with the surrounding sparsely crosslinked regions, resulting in stress concentration points. Additionally, excessive chain entanglement restricts segmental motion, hindering further double bond conversion (reducing the effective crosslinking density) and inhibiting the dynamic exchange of disulfide bonds. To further verify the role of UV-curing in constructing the crosslinking network, the mechanical properties of the uncured specimen (PUU-SS25%-uncured) were tested. The specimen was extremely soft and weak, with a tensile strength of only 1 MPa, indicating that an effective crosslinked structure had not yet formed inside the material. After UV curing, the acryloyl double bonds undergo radical polymerization, forming a stable covalent crosslinking network inside the material. This transforms the material from a linear oligomer into a three-dimensional network elastomer, thereby endowing it with excellent properties, such as high resilience and toughness.

As observed in Fig. 3(b), Zn^{2+} forms metal coordination bonds with the nitrogen/oxygen atoms in the polymer backbone. At 1 wt% $ZnCl_2$, these non-covalent coordination interactions enhance both tensile strength (from 6.41 MPa to 11.18 MPa) and elongation at break (from 1198% to 2423%), with toughness increasing from 39.25 MJ/m^3 to 129.95 MJ/m^3. The coordination bonds act as sacrificial bonds, preferentially breaking under tension to dissipate energy and protect the main chain network, whereas their dynamic reversibility allows recombination after deformation, improving fatigue resistance.[2,17] However, excessive $ZnCl_2$ leads to overly dense coordination bonds that restricts segmental motion and inhibited disulfide bond exchange, resulting in no property improvement. As shown in Fig. 3(c), at low strain

(Region I), the metal coordination bonds and hydrogen bonds are not significantly activated, and the material exhibits linear elastic behavior. As the strain increases (Region II), Zn^{2+} coordination bonds preferentially break as sacrificial crosslinks, whereas hydrogen bonds undergo reversible dissociation and synergistically dissipate strain energy. Under large strain (Region III), hydrogen bond dissociation approaches saturation, disulfide bonds undergo dynamic exchange, and the covalent main chain bears the primary stress, achieving an ultrahigh elongation of 2423%.[11] As the Cy content increases, the proportion of dynamic disulfide bonds in the PUU-SS system increases, while the crosslinking density exhibits a gradual decreasing trend (the crosslinking density of the PUU-SS25% sample is only 0.62×10^{-5} mol·cm^{-3}, with an elastic modulus of 463.79 kPa). The decrease in the elastic modulus enables the material to undergo larger deformation under lower external forces (see Table S3 in ESI), significantly improving its flexibility and deformation adaptability. Meanwhile, the reduction in crosslinking density diminishes the constraints of permanent chemical crosslinking points, enhances the mobility and rearrangement capability of molecular chain segments, and allows the material to recover its initial shape more quickly after being stressed, thereby greatly increasing its resilience.[27,28] Fig. 3(d) shows the DSC curves of PUU-SS25% and PUU-SS25%-Zn1wt%, with T_g values of 1.83 and 4.33 °C, respectively. Sharp melting peaks are not observed, indicating an amorphous structure. The increase in T_g suggests that Zn^{2+} forms metal coordination bonds with the backbone N/O atoms, acting as physical crosslinks that restrict chain mobility. Figs. S3(b) and S3(c) (in ESI) show that as the Cy content increases from 0% to 30%, the Shore hardness continuously decreases (from 74.28 to 62.57). The Shore A hardness of the material before and after modification remains approximately 60, rendering it suitable for use as a substrate in wearable devices.

High Resilience of PUU-SS25%-Zn1wt% Elastomer

As shown in Fig. 4(a), PUU-SS25%-Zn1wt% and PUU-SS25% were stretched to 100%, 500%, and 1000% strains (Fig. 4c and Figs. S4a–S4e in ESI) and then rapidly unloaded. At 100% and 500% strain, PUU-SS25%-Zn1wt% exhibited excellent resilience, recovering its original length within 5 s after 500% strain, with a recovery rate exceeding 93% after multiple cycles (Figs. 4c and 4d). This was because the PCDL soft segments were randomly entangled before stretching and retracted entropically upon unloading. Although this leads to a lower tensile strength than that of some special polyurethanes, the flexibility and resilience are greatly enhanced. As observed in Fig. 4(b), PUU-SS25%-Zn1wt% achieved an elastic recovery rate of 99.6% after the first unloading from 1000% strain and 90.2% after five cycles (Fig. S4g in ESI). In contrast, PUU-SS25% fractured after two cycles at 1000% strain (Fig. S4c in ESI). This indicates that Zn^{2+} acts as a sacrificial bond that synergizes with hydrogen bonds, preferentially breaking before covalent and disulfide bonds and rapidly recombining during rest, thereby protecting the main chain network. In Fig. S4(d) (in ESI), the initial stress of the material is 4 MPa, which then decreases to 2.59 MPa before rising back to 4.8 MPa. To reveal the contribution of dynamic bonds (disulfide and

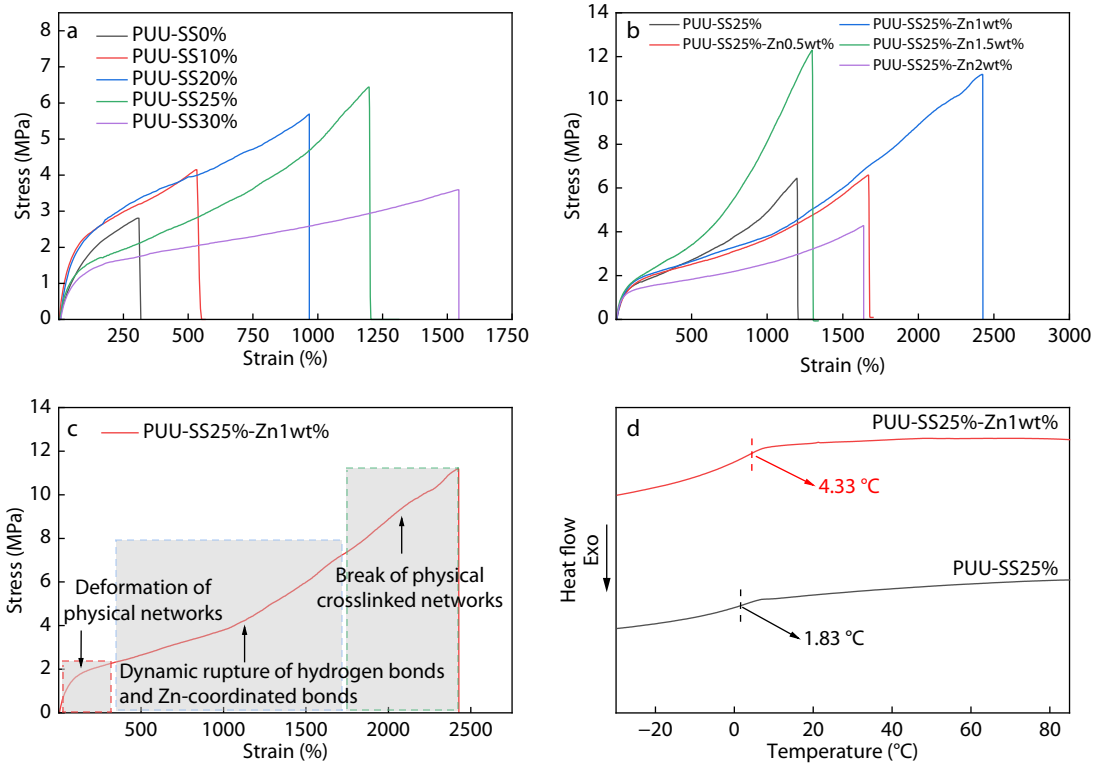

Fig. 3 (a) Stress-strain curves of UV-curing polyurethanes with varying Cy contents; (b) Stress-strain curves of PUU-SS25% with varying $ZnCl_2$ coordination contents; (c) Covalent crosslinking network and metal coordination self-reinforcing mechanism of PUU-SS25%-Zn1wt%; (d) DSC thermograms of PUU-SS25% and PUU-SS25%-Zn1wt%.

https://doi.org/10.1007/s10118-026-3782-7

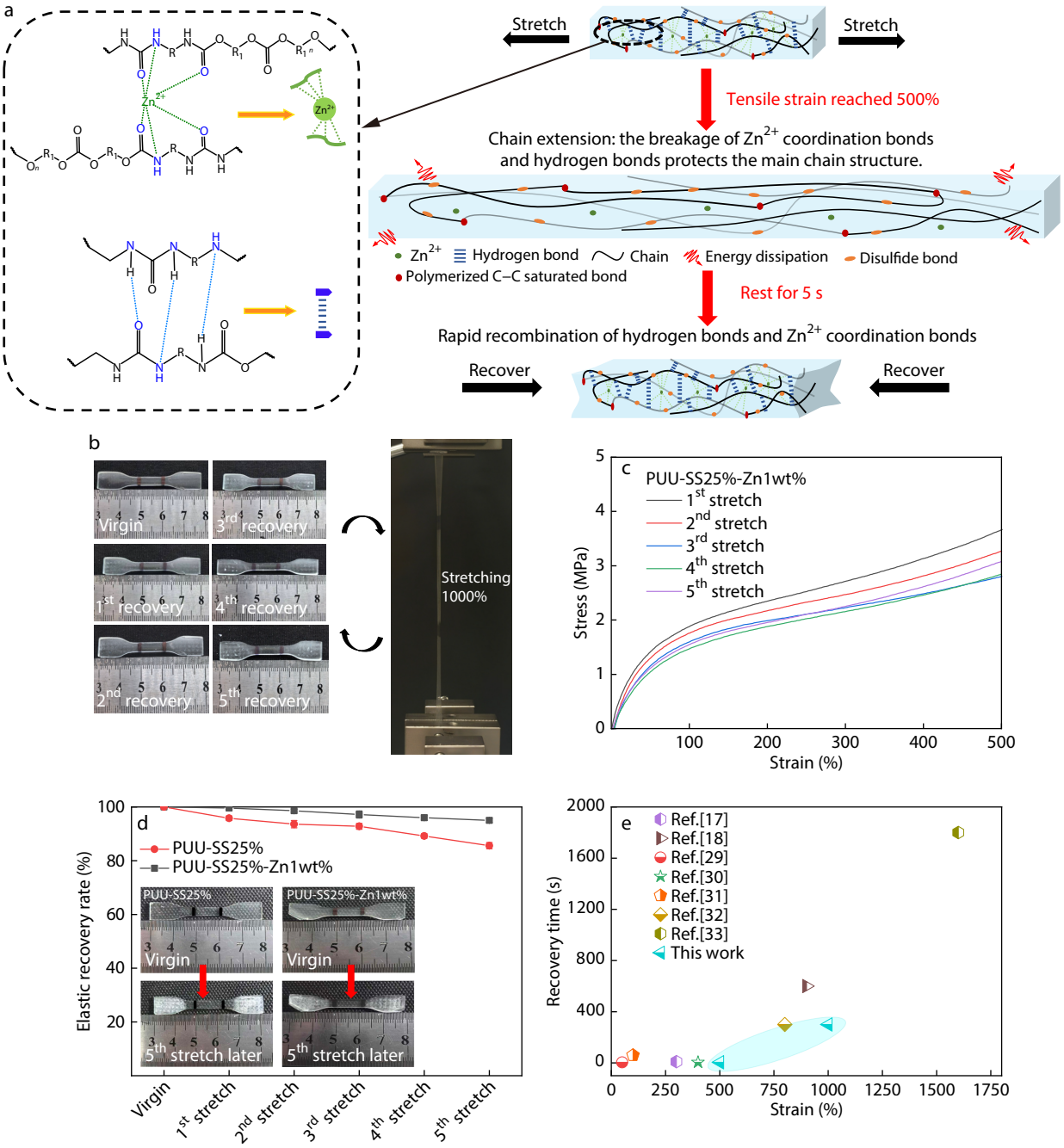

Fig. 4 (a) Tensile resilience behavior of the PUU-SS25%-Zn1wt% elastomer; (b) Photographs of the effective gauge length after stretching to 1000% strain followed by immediate release and 5 min of rest; (c) Stress-strain curves of PUU-SS25%-Zn1wt%; (d) Elastic recovery rate of PUU-SS25%-Zn1wt% after 500% strain; (e) Statistical comparison of tensile strain and recovery time between this work and reported polyurethanes[17,18,29–33]

Zn^{2+} coordination bonds) to the dynamic mechanical behavior and resilience of the polyurethane-urea elastomer, a permanent crosslinked control sample (PUU-CC25%) was prepared using hexamethylenediamine (HDA) as a chain extender without disulfide bonds. By comparing the frequency-dependent storage modulus (E') and loss modulus (E'') of the two samples under identical DMA frequency sweep conditions, this study elucidates how dynamic bonds regulate the frequency dependence, energy dissipation, and their intrinsic relationship with high resilience and fatigue resistance.

As evidenced by Fig. S5(a) (in ESI), in the DMA frequency sweep (0.1–50 Hz), compared with the permanent crosslinked control, PUU-SS25%-Zn1wt% exhibited a smaller increase in the storage modulus (E') but a larger increase in the loss modulus (E'') with frequency. The former is attributed to the dynamic reversibility of Zn^{2+} coordination and disulfide bonds, which partially dissipate energy *via* rapid recombination at high frequencies, slowing network hardening, and maintain-

ing flexibility across a wide frequency range. The latter indicates that bond breakage-recombination introduces additional energy dissipation, particularly at higher frequencies. This dynamic response directly demonstrates high resilience. At low frequencies (service conditions), dynamic bonds fully recombine, resulting in a low loss factor ($\tan\delta = E''/E'$).[34] Most of the strain energy is elastically released upon unloading, achieving a 99.6% recovery. Under high-frequency impact, dynamic bonds act as sacrificial crosslinks, rapidly dissipating energy and protecting the network from irreversible damage, ensuring stable large-strain resilience, outperforming the polyurethane elastomers reported in Fig. 4(e). Thus, DMA reveals the inherent behavior of the dynamic bonds in PUU-SS25%-Zn1wt%, exhibiting low loss at low frequencies and high dissipation at high frequencies,[35–37] which is the intrinsic origin of its high resilience. As illustrated in Figs. S5(b) and S5(c) (in ESI), the relaxation time of PUU-SS25%-Zn1wt% follows the Arrhenius equation. From the linear fit of ln(τ) versus 1000/T, the relaxation activation energy is determined to be 60.2 kJ/mol. A low activation energy (<40 kJ/mol) causes frequent bond breakage at room temperature, leading to network relaxation and poor mechanical properties.[38] A high activation energy (>100 kJ/mol) hinders bond activation, reduces self-healing efficiency, and requires high processing temperatures.[32] The moderate activation energy of the polyurethane elastomer in this study ensured the structural integrity of the material network and its high resilience at room temperature. Notably, when the temperature was increased to 110 °C, the relaxation time decreased sharply, indicating that under thermal or mechanical stimulation, the dynamic bonds responded rapidly through reversible breakage and recombination. Furthermore, the thermogravimetric analysis (TGA) results in Figs. S6(a) and S(b) (in ESI) show that the PUU-SS25%-Zn1wt% elastomer exhibits good thermal stability, with a 5% weight loss temperature ($T_{5\%}$) of 296.68 °C and a maximum decomposition rate temperature (T_{max}) of 350.83 °C (Table S4 in ESI). The $T_{5\%}$ value is significantly higher than those of conventional polyether- or polyester-based polyurethanes[39–41] (typically 230–260 °C), which is attributed to the thermally stable polycarbonate soft segment,[42] the crosslinked network structure, and the synergistic effects of the dynamic bonds. After adding 1 wt% $ZnCl_2$, PUU-SS25%–Zn1wt% exhibited superior tensile properties, toughness, resilience, and fatigue resistance. Cyclic tensile tests were conducted to investigate the energy dissipation from multiple hydrogen bonds, disulfide bonds, UV-cured covalent networks, and metal coordination bonds and to verify their resilience. After 100 cycles at 500% strain (Fig. 5a), the energy dissipation decreased with the cycle number. Following an initial drop from 4.395 MJ/m^3 (1st cycle) to 1.82 MJ/m^3 (2nd cycle), which is due to irreversible breakage of unfavorably positioned disulfide bonds and disruption of ordered hydrogen bonds, the energy dissipation stabilizes through the synergy between the UV-cured covalent network and the metal coordination network. Even after 100 cycles, the material retained 0.832 MJ/m^3 (18.93% of its initial value), demonstrating a good energy dissipation capacity under large-strain cycling. This sustained energy dissipation confirms the re-

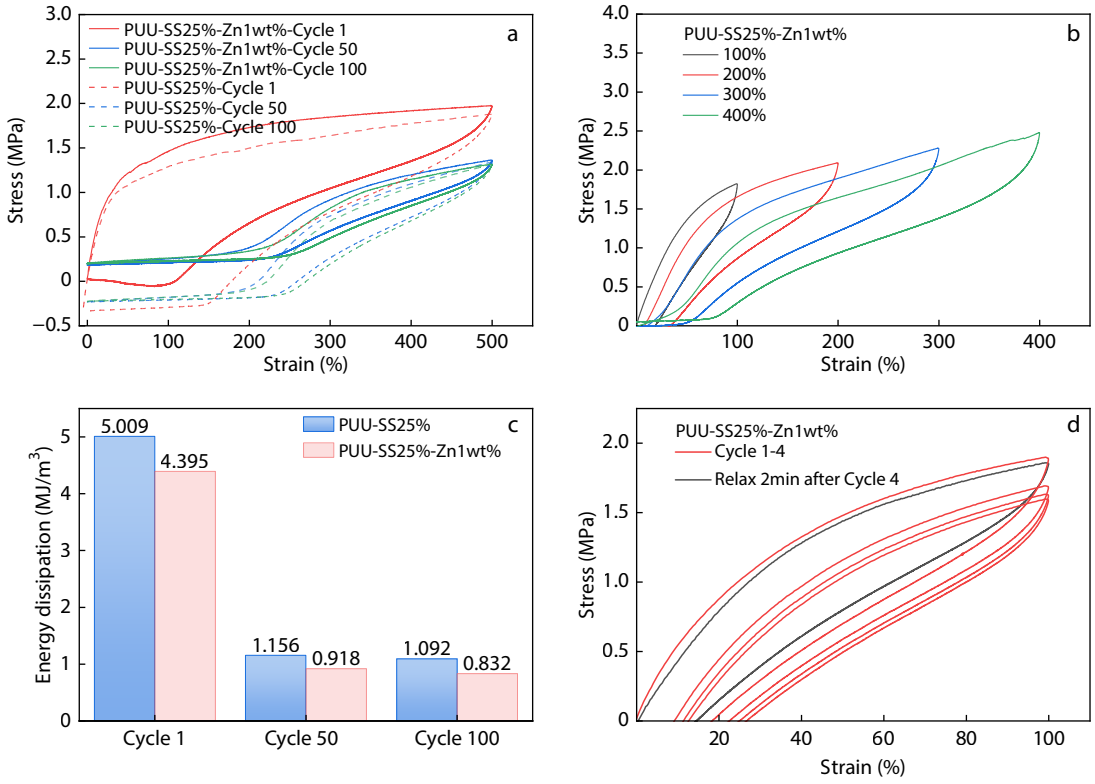

Fig. 5 (a) Stress-strain cyclic curves of PUU-SS25% and PUU-SS25%-Zn1wt%; (b) Cyclic tensile curves at four strains of PUU-SS25%-Zn1wt%; (c) Comparison of energy dissipation between PUU-SS25% and PUU-SS25%-Zn1wt%; (d) Stress-strain cyclic curves of PUU-SS25%-Zn1wt% after 2 min of rest.

versibility of hydrogen, disulfide, and metal coordination bonds, which continuously break and recombine during large cyclic deformations. It also demonstrates excellent fatigue resistance because the network maintains its structural integrity under repeated loading. As the strain increased from 100% to 400% (Fig. 5b), both the hysteresis loop area and dissipated energy gradually increased. The addition of $ZnCl_2$ reduces the residual strain and dissipated energy during cycling, because the metal coordination bonds protect the hard-segment hydrogen bond network. During stretching, the coordination bonds act as sacrificial crosslinks that preferentially absorb strain energy, thereby shielding hydrogen bonds from extensive disruption. Moreover, the rapid recombination of Zn^{2+} coordination bonds upon unloading achieves efficient elastic energy recovery, resulting in a higher unloading curve and a smaller hysteresis loop.

Thus, the Zn^{2+} coordination network dissipates less energy while maintaining excellent elastic recovery, demonstrating the synergistic advantage of integrating metal coordination bonds into the dynamic network architecture (Fig. 5c). Remarkably, the PUU-SS25%-Zn1wt% elastomer exhibits the ability to recover from large strain without external intervention (Fig. 5d). When the rest time between the fourth and fifth cycles was set to 2 min, the residual strain and hysteresis energy almost completely recovered, as shown by the overlapping loading-unloading curves. The rapid recovery of the specimen dimensions and mechanical properties is attributed to the reconstruction of weak hydrogen bonds and coordination bonds disrupted by the applied force.

Self-healing Performance of PUU-SS25% and PUU-SS25%-Zn1wt% Elastomer

Different amounts of Cy and $ZnCl_2$ endow PUU-SS*x*%–Zn*y*wt% elastomers with abundant reversible hydrogen bonds, disulfide bonds, and metal coordination bonds,[43,44] thereby exhibiting excellent self-healing performance (Figs. 6d–6f). Long-chain molecules easily approach each other under thermal motion,

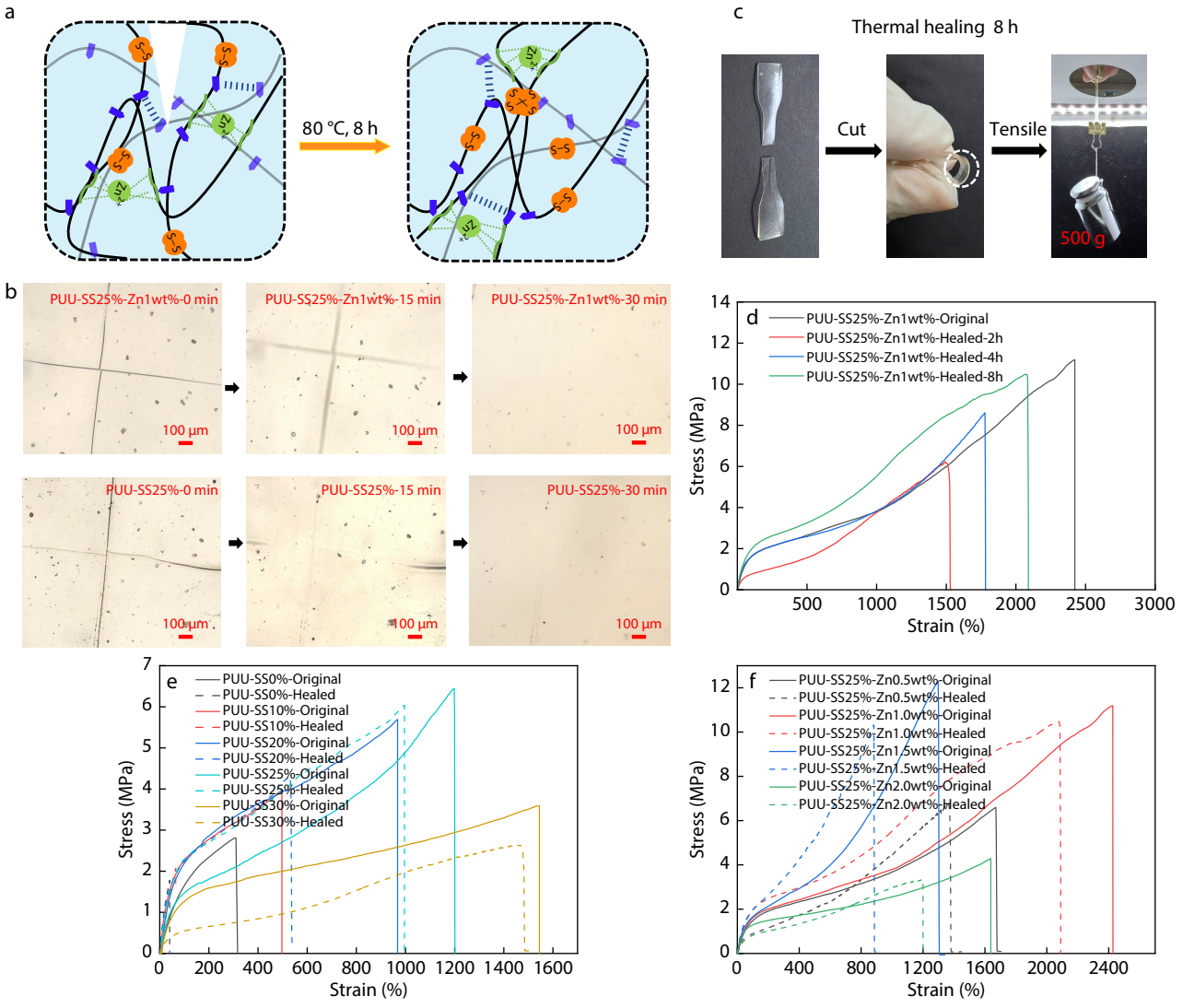

Fig. 6 (a) Disulfide bonds exchange, and coordination/hydrogen bonds recombine; (b) Metallographic microscope images of PUU-SS25%-Zn1wt% and PUU-SS25% films with artificially created cross-shaped scratches before thermal healing; (c) Self-healing performance of PUU-SS25%-Zn1wt% lifting a 500 g weight; (d) Stress-strain curves of self-healing PUU-SS25%-Zn1wt% elastomer; (e) Stress-strain curves of self-healing PUU-SS*x*% elastomers; (f) Stress-strain curves of self-healing PUU-SS25%-Zn*y*wt% elastomers.

https://doi.org/10.1007/s10118-026-3782-7

forming dense and reversible hydrogen-bonding networks. Under thermal stimulation, disulfide bonds undergo reversible metathesis reactions, enabling covalent network reconnection across the fractured interface *via* disulfide bond exchange.[45,46] Meanwhile, the synergistic breakage and recombination of hydrogen and metal coordination bonds further accelerate the interfacial healing process (Fig. 6a). The synergy of these three dynamic bonds enables PUU-SS25%-Zn1wt% to achieve a self-healing efficiency of 93% at 80 °C, which is attributed to the recombination of disulfide bonds[47] and rapid reversible recombination of hydrogen and metal coordination bonds.[48] Although the healed strength was high, the elongation at break decreased, indicating a coordinated healing mechanism. Fig. 6(b) shows optical images of the PUU-SS25%-Zn1wt% and PUU-SS25% films before and after healing. Fig. 6(c) demonstrates that the healed elastomer can lift a 500 g weight without breaking, indicating excellent post-healing mechanical performance and the potential to reduce the replacement frequency of key components.

CONCLUSIONS

In this study, a UV-curable polyurethane-urea elastomer (PUU-SS25%-Zn1wt%) is fabricated based on dual crosslinked networks of multiple hydrogen bonds, disulfide bonds, and Zn^{2+} coordination bonds. Cy introduces urea linkages and disulfide bonds, $ZnCl_2$ constructs metal coordination bonds, and HEA end-capping enables rapid UV curing (100 s). This synergy enables the material to achieve high resilience (complete recovery within 5 s at 500% strain and 99.6% recovery at 1000% strain), high toughness (2423% elongation, 129.95 MJ/m^3), and moderate-temperature self-healing (93% efficiency and scratches heal within 30 min at 60 °C). The material also exhibits a high transparency (>92%) and flexible substrate characteristics. This work reveals the intrinsic relationships among crosslinking density, dynamic bond mobility, and mechanical properties, offering a new strategy for designing UV-curable polyurethane-urea elastomers with rapid curing, high resilience, and self-healing for flexible electronics, wearable sensors, and biomedical engineering.

Conflict of Interests

The authors declare no interest conflict.

Electronic Supplementary Information

Electronic supplementary information (ESI) is available free of charge in the online version of this article at http://doi.org/10.1007/s10118-026-3782-7.

Data Availability Statement

The data supporting the findings of this study are available from the corresponding author upon reasonable request.

ACKNOWLEDGMENTS

This work was financially supported by the National Natural Science Foundation of China (No. 52273104).

REFERENCES

1 Liang, K.; Qi, X. K.; Xiao, X.; Wang, L.; Zhang, J. L. Chemically-informed active learning enables data-efficient multi-objective optimization of self-healing polyurethanes. *Chem. Sci.* **2026**, *7*, 3627−3638.
2 Tu, Z. K.; Liu, W. F.; Wang J.; Qiu, X. Q.; Huang, J. H.; Li, J.X.; Lou, H. M. Biomimetic high performance artificial muscle built on sacrificial coordination network and mechanical training process. *Nat. Commun.* **2021**, *12*, 2916.
3 Ng, W. W.; Chen, W. H.; Thiam, H. S.; Lim, S.; Chih, Y. K.; Pang, Y. L. A review of self-healing mechanisms for the application of conductive electronic products. *RSC Adv.* **2026**, *16*, 9666−9681.
4 Xu, C.; Ma, X. L.; Sun, Y.; Shang, J. L.; Sun, S. P.; Yang, L.; Zhang, W.; Xue, D. C.; Zhu, Y. Q.; Li, X. D.; Jiang, H.; Cao, C. B. Su, X.; Zou, M.S. Polyurethane elastomer with unprecedented thermostability, long-cycle antifatigue, and ultrafast self-healing capability. *Small.* **2025**, *21*, e05297.
5 Jang, H.; Lee, J.; Beak C. J.; Biswas, S.; Lee, S. H.; Kim H. Flexible neuromorphic electronics for wearable near-sensor and in-sensor computing systems. *Adv. Mater.* **2025**, *37*, 2416073.
6 Hamidi A.; Tadesse Y. 3D printing of very soft elastomer and sacrificial carbohydrate glass/elastomer structures for robotic applications. *Mater. Des.* **2020**, *187*, 108324.
7 Yang, M.; Peng, K.; Li, Z.; Gao, Y.; Tian, Q.; Zhou, Z.; Chen, Y. Recent progress in flexible materials for wearable devices for body function and athletic performance monitoring. *Chem. Eng. J.* **2025**, *505*, 159659.
8 Wang, W.; Li, Y.; Ma, Z.; Chen, Q.; Zhang, W.; Yang, T.; Sun, J. Ultra-tough poly(urea-urethane) plastics with superior impact resistance for cryogenic applications. *Adv. Mater.* **2025**, *37*, 2509421.
9 Yue, L.; Wan, X.; Turel, T.; Schenning, A. P.; Tomovic, Z.; Debije, M. G. Responsive industrial polymers: a marriage of polyurethanes with liquid crystal elastomers *ACS Appl. Mater. Interfaces* **2025**, *17*, 31685−31697.
10 Wang, D.; Wang, Z.; Ren, S.; Xu, J.; Wang, C.; Hu, P.; Fu, J. Molecular engineering of a colorless, extremely tough, superiorly self-recoverable, and healable poly(urethane-urea) elastomer for impact-resistant applications. *Mater. Horiz.* **2021**, *8*, 2238−2250.
11 Zhang, K.; Chen, J.; Shi, X.; Qian, H.; Wu, G.; Jiang, B.; Huang, Y. Bioinspired self-healing and robust elastomer *via* tailored slipping semi-crystalline arrays for multifunctional electronics. *Chem. Eng. J.* **2023**, *454*, 139982.
12 Zhao, J. J.; Sun, S. B.; He, S. H.; Wu, Q.; Shi, F. Catalytic asymmetric inverse-electron-demand oxa-diels-alder reaction of in situ generated ortho-quinone methides with 3-methyl-2-vinylindoles. *Angew. Chem. Int. Ed.* **2015**, *54*, 5460−5464.
13 Cao, M.H.; Green, N.J.; Xu, S.Z. Application of the aza-diels-alder reaction in the synthesis of natural products. *Org. Biomol. Chem.* **2017**, *15*, 3105−3129.
14 Du, Q.; Wu, P.; Sun, S. Damage-tolerant stretchable ionic conductors. *Fundam. Res.* **2025**, *5*, 2850−2861.
15 Li, Y.; Zhou, M.; Wang, R.; Han, H.; Huang, Z.; Wang, J. Self-healing polyurethane elastomers: an essential review and prospects for future research. *Eur. Polym. J.* **2024**, *214*, 113159.
16 Huang, W.; Zu, Z.; Huang, Y.; Xiang, H.; Liu, X. UV-curing 3D printing of high-performance, recyclable, biobased photosensitive resin enabled by dual-crosslinking networks. *Addit. Manuf.* **2024**, *91*, 104352.
17 Wang, S.; Chen, X.; Guo, L.; Wang, S.; Dong, F.; Liu, H.; Xu, X. A human muscle-inspired, high strength, good elastic recoverability, room-temperature self-healing, and recyclable

Graphical Abstract

Self-healing, High-resilience, and UV-curable Polyurethane-urea Elastomers Enabled by Dual Crosslinked Networks

Meng-Yuan Cai, Sao Su, Wen-Tao Du, Rui-Jie Xu, and Hong-Ping Xiang

Guangdong University of Technology

In this study, we developed a novel UV-curable polyurethane-urea elastomer containing disulfide, hydrogen, and metal coordination bonds. It can be rapidly UV-cured within 100 s, exhibiting ultrahigh resilience (99% recovery at 1000% strain) and excellent self-healing efficiency (93% at 80 °C), providing an effective strategy for high-performance flexible electronics.

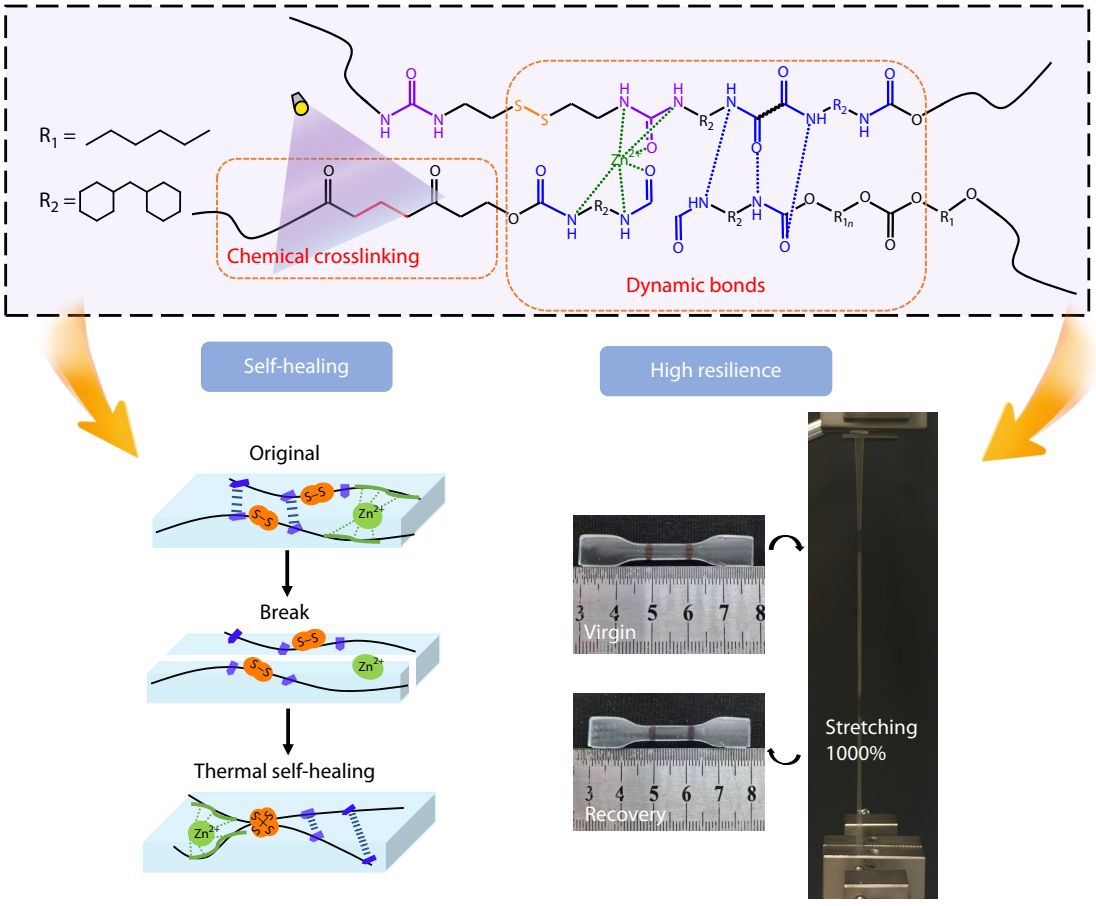

Chinese J. Polym. Sci., 2026 *https://doi.org/10.1007/s10118-026-3782-7*

polyurethane elastomer based on dynamic bonds. *Compos. Sci. Technol.* **2024**, *248*, 110457.

18 Xu, Y.; Zhou, S.; Wu, Z.; Yang, X.; Li, N.; Qin, Z.; Jiao, T. Room-temperature self-healing and recyclable polyurethane elastomers with high strength and superior robustness based on dynamic double-crosslinked structure. *Chem. Eng. J.* **2023**, *466*, 143179.

19 Gao, H.; Huang, X.; Arockiyasamy, A. R.; Zhou, X.; Ding, X.; Zheng, L.; Wu, L. Vat photopolymerization of stretchable foam with highly entangled and crosslinked structures. *Nat. Commun.* **2025**, *16*, 4756.

20 Zhang, H.; Shang, Y.; Li, N.; Hu, X.; Ye, Z.; Zhang, X.; Shi, B. Dynamic bond-enhanced, recyclable polyurethane elastomer with high strength and self-healing properties for advanced 3D printing. *Compos. Part B.* **2025**, *304*, 112500.

21 Tian, X.; Sun, Y.; Wang, T.; Duan, T.; Guo, H.; Su, H.; Gao, G. UV-curable silane-modified polyurethane acrylate with high stretch ability and sensitivity for flexible sensors. *ACS Appl. Polym. Mater.* **2026**, *8*, 3996−4006.

22 Meng, Y.; Liu, J.; Li, J.; Gao, Y.; Zhang, Z. Preparation and

characterization of the cross-linked fluoro-silicon polyacrylate-polyurethane hybrid emulsions for superior performance of waterborne coatings. *ACS Appl. Polym. Mater.* **2023**, *5*, 7854−7866.
23 Zhang, Q. H.; Xie, Z. X.; Pang, Y. J.; Xiang, H.P. Upcycling thermosetting polysiloxanes into thermoplastics *via* UV-induced surface photopolymerization of acrylates. *Chem. Commun.* **2026**, *62*, 4085−4088.
24 Zhang, Z. H.; Ye, J.; Wen, W. S.; Luo, Q. H.; Xiang, H. P. UV-curable, transparent, and low volume-shrinkage silicones for efficient mini-LED encapsulation. *Chinese J. Polym. Sci.* **2026**, *44*, 599−610.
25 Jin, H.; Zhong, X.; Zhong, C.; Dai, W.; Xiang, H. P.; Zhang, L. Y. UV-curable, 3D printable, thermally conductive polysiloxane composites for thermal interface devices. *Addit. Manuf.* **2025**, *99*, 104658.
26 Peng, S.; Li, Y.; Wu, L.; Zhong, J.; Weng, Z.; Zheng, L.; Miao, J. T. 3D printing mechanically robust and transparent polyurethane elastomers for stretchable electronic sensors. *ACS Appl. Mater. Interfaces*. **2020**, *12*, 6479−6488.
27 Peng, J. J.; Zhang, Y. Modification of Octavinyl POSS and Its Effect on the Mechanical Properties and Thermal Stability of Silicone Rubber/POSS Composites. *Nanomaterials* **2025**, *15*, 1706.
28 Valizadeh, I.; Tayyarian, T. Weeger O. Influence of process parameters on geometric and elasto-visco-plastic material properties in vat photopolymerization. *Addit. Manuf.* **2023**, *25*, 103641.
29 Ning, C.; Gong, D.; Wu, L.; Chen, W.; Zhang, C. Preparation of gradient polyurethane and its performance for flexible sensors. *Polymers* **2024**, *16*, 1617.
30 Tian, C.; Zhao, F.; Yang, N.; Jiang, Y.; Huang, L.; Zhou, F.; Cai, X. Durable, super-resilient, and ultra-strong polyurethane elastomers *via* a dense hydrogen bond cross-linking strategy. *Macromolecules* **2025**, *58*, 2905−2916.
31 Zheng, K.; Guo, A.; Li, X.; Lin, Y.; Zhang, S.; Yang, R.; Sui, C. Ultra strong and tough bio-based polyurethane elastomers with rigid-flexible hybrid soft segment supramolecular cross-linked networks. *Adv. Funct. Mater.* **2026**, *36*, e09794.
32 Wang, L.; Zhang, K.; Zhang, X.; Tan, Y.; Guo, L.; Xia, Y.; Wang, X. Mismatched supramolecular interactions facilitate the reprocessing of super-strong and ultratough thermoset elastomers. *Adv. Mater.* **2024**, *36*, 2311758.
33 Qian, Y.; Dong, F.; Wang, S.; Jiang, Y.; Xu, X.; Liu, H. Ultrarobust, stretchable, and highly elastic supramolecular elastomer with hydrogen-bond interactions *via* sp2 hybridized boron-urethane bonds. *Angew. Chem. Int. Ed.* **2025**, *64*, e202421099.
34 Pang, J.; Zhong, J.; Pu, Z.; Yang, K.; Yang, Y.; Yue, M.; Wu, L. Study on synthesis of polycarbonate dilate polyurethane elastomers. *J. Polym. Res.* **2024**, *31*, 149.
35 Pei, P.; Du, Y.; Miao, Y.; Suo, T. Novel hyper-viscoelastic approach to modelling elastomer mechanic behaviour with relaxation spectrum. *Polym. Test.* **2024**, *133*, 108375.
36 Jeong, J. H.; Kim, H. J.; Choi, Y. H.; Song, G. S.; Yoo, S. I.; Eom, Y. Effects of preparation routes on the physical and rheological properties of isosorbide-based thermoplastic polyurethanes. *Macromol. Res.* **2023**, *31*, 133−142.
37 Zhang, J. W.; Li, J.; Huang, C. H.; Chen S. Study on dynamic viscoelastic constitutive model of nonwater reacted polyurethane grouting materials based on DMA. *Rev. Adv. Mater. Sci.* **2022**, *61*, 238−249.
38 Bai, K. N.; Xie, C. H.; Liu, W. T.; You, Y.; Li, Y. Q. Big data approach to explore the activation energy from stress-relaxation of polyurethane vitrimers. *Acta Polymerica Sinica* (in Chinese) **2025**, *56*, 1621−1632.
39 Li, Y.; Zhang, B.; Zhao, Y.; Lu, S.; Fan, D.; Wang, S.; Li, S. Synthesis and characterization of cardanol-based non-isocyanate polyurethane. *Polymers* **2023**, *15*, 4683.
40 Futter, J.; Richter, L. F.; Hörl, S.; Kränzlein, M.; Rieger, B. Coordinative ring-opening polymerization of limonene carbamate toward phosgene- and isocyanate-free polyurethane. *Angew. Chem. Int. Ed.* **2025**, *64*, e202502727.
41 Lubczak, J. Derivatization of PVA into polyols suitable for fabrication of rigid polyurethane foams-preliminary studies and perspectives. *Materials* **2025**, *18*, 2780.
42 Zhao, C. Y.; Wang, C. X.; Wang, Y. J.; Yao, D. G. Super stretchable chromatic polyurethane driven by anthraquinone chromogen as a chain extender. *RSC Adv.* **2019**, *9*, 2332−2342.
43 Zu, Z. J.; Cao, Y. Y.; Liu, J. W.; Lin, Z. Q.; Zhang, L. Y.; Xiang, H. P.; Zhang, M. Q. Self-healing, reprocessable, and antibacterial silicone rubber enabled by ionic crosslinking bonds. *Acta Polymerica Sinica* (in Chinese) **2025**, *56*, 152−165.
44 Ye, J.; Zu, Z. J.; Lin, Z. Q.; Xiang, H. P.; Zhang M. Q. Intrinsic self-healing polysiloxane materials: From single dynamic crosslinked network to multiple dynamic crosslinked networks. *Acta Polymerica Sinica* (in Chinese) **2023**, *54*, 1028−1054.
45 Shi, H. L.; Shi, Y.; Ren L.P.; Zhang, W.; Ji, Y.; Zhang, J. C.; Zhong, X. ; Liang, Y. L. ; Dong, J. D. ; Wu, Y. D. ; Li, W. ; Zhang, D. W.; Jiang, Z. X. A self-reinforcing, self-healing, and shape memory polybutadiene-based polyurethane *via* disulfide bonds for healable flexible sensors. *Chem. Eng. J.* **2025**, *511*, 161524.
46 Canadell, J.; Goossens, H.; Klumperman, B. Self-healing materials based on disulfide links. *Macromolecules* **2011**, *44*, 2536−2541.
47 Tian, Y.; Wei, Y.; Wang, M.; Wang, J.; Li, X.; Qin, X.; Zhang, L. Ultra-stretchable, tough, and self-healing polyurethane with tunable microphase separation for flexible wearable electronics. *Nano Energy* **2025**, *139*, 110908.
48 Zhang, M.; Wang, Y.; Yang, M.; Deng, Y.; Zhou, W.; Wang, H.; Chen, Y. Fabrication of mechanical strong supramolecular waterborne polyurethane elastomers with the inspiration of hierarchical dynamic structures of scallop byssal threads. *Adv. Funct. Mater.* **2025**, *35*, 2413083.